Deposition and Characterization of Copper Chalcopyrite Based Solar Cells using Electrochemical Techniques

P. J. Dale[a], A. P. Samantilleke[a], G. Zoppi[b], I. Forbes[b], S. Roncallo[c], and L. M. Peter[a]

[a] Department of Chemistry, University of Bath, BA2 7AY, UK
[b] Northumbria Photovoltaics Applications Centre, Northumbria University, NE1 8ST, UK
[c] Centre for Materials Science & Engineering, Cranfield University, SN6 8LA, UK

$Cu(In,Ga)Se_2$ films were electrodeposited on molybdenum substrates from a single pH buffered bath and annealed in a reducing selenium atmosphere. The opto-electronic properties of the films were characterized using a potentiostatically-controlled three electrode setup and an electrolyte contact. Pulsed illumination was used to determine the carrier type and the speed of photoresponse. Chopped monochromatic illumination was used to measure photocurrent spectra. The electrodeposited copper chalcopyrite films were compared with films prepared by sputtering and spraying techniques. All electrodeposited films gave p-type photoresponses, and the sputtered film had the highest photocurrent. Optimum cyanide etch times to illicit the maximum photocurrent response were different for each material. The band gap of electrodeposited $CuInSe_2$ was 0.95 eV, which was slightly lower than that of the sputtered film. The electrodeposited $Cu(In,Ga)Se_2$ material gave a smaller photo-response but its band gap appeared to be similar to that of $CuInSe_2$. The best device based on an electrodeposited absorber layer had an efficiency of 4.5 %.

Introduction

Thin film copper chalcopyrites ($CuIn(Ga)(Se,S)_2$) are used as absorber materials for second generation photovoltaic devices, and have shown laboratory efficiencies of up to 19.5% (1). Commercially, the majority of the absorber layers are manufactured using sputtering techniques followed by annealing in the presence of a chalcogen (selenium and/or sulfur) (2). Electrodeposition is a low energy technique that was successfully used by BP Solar to make semiconductor grade CdTe absorber layers in its commercially realized solar cells (3). Several approaches have been taken to electrodeposit copper chalcopyrite absorber layers, such as one step electrodeposition of all the elements by constant potential (4, 5) or pulsed potential (6), electrodeposition of the metal alloys (7), or electrodeposition of the individual metals (8). In all cases re-crystallization of the as-deposited films by thermal annealing is required to form suitable photovoltaic material. Lincot *et al*. have reported a one step electrodeposition technique, where the deposition process is controlled by mass transport and have shown that electrodeposited $CuInSe_2$-based absorber layers, which are subsequently re-crystallized in the presence of sulfur, can give device efficiencies of 11.3% (5). Calixto *et al.* have used a pH buffer to assist gallium incorporation into the films, but this buffer may have secondary effects as it

appears to reduce hydrogen evolution at the deposition surface, and reduces the deposition flux (4).

Examination of the opto-electronic properties of the copper chalcopyrite layers without the need for cell fabrication is possible by using a liquid electrolyte to contact the front of the layer and the molybdenum substrate to contact the back of the layer. The advantage of doing this is that there is no requirement to complete to a full device before examining the absorber properties, although other processing steps or layers needed to complete the photovoltaic device may of course affect the absorber layers properties. Electrolyte contacts are easy to apply and remove and the redox level can be readily altered by an appropriate choice of redox couple. Using an electrolyte contact to examine the photocurrent of an absorber layer also provides a quick screening method to determine whether the layers are of sufficient quality to use for making photovoltaic devices. Chen *et al.* (9) identified that any electrolyte contact should be inert with respect to the chalcopyrite film, and that it should have a suitable redox couple in order to observe photoeffects. For this purpose they identified a cobalt complex in an organic solvent in oxygen free conditions as suitable for studying single crystal and evaporated layers of $CuInSe_2$. Other groups have used a vanadium redox couple to study the properties of $CuInS_2$ (10), or polysulfide electrolytes to study n-type $CuInSe_2$ films (11). Lincot *et al.* have reported that aqueous solutions containing europium (III) ions are suitable for measuring current and capacitance voltage data as well as photocurrent spectra for $CuInSe_2$ layers (12). Lincot and others (13-14) have also used photocurrent spectra measurements as a measure of quality of their films as well as a diagnostic tool for examining 'dead layers' that some $CuInSe_2$ films develop after annealing .

In the present work we have electrodeposited $Cu(In,Ga)Se_2$ films using a modification of the protocol developed by Calixto *et al.* (4). The films were characterized by photovoltammetry, photocurrent transients, and photocurrent spectroscopy. These measurements were used to determine optimum cyanide etch times for the films. Comparisons were made with copper chalcogenide materials deposited using vacuum and spray methods.

Method

$Cu(In,Ga)Se_2$ films were electrodeposited at room temperature onto molybdenum coated glass slides from a 250 ml pH 3 buffered aqueous solution containing 2.6 mM $CuCl_2$, 9.6 $InCl_3$, 5.5 mM H_2SeO_3 and 240 mM LiCl for $CuInSe_2$ and 2.56 mM $CuCl_2$, 2.4 mM $InCl_3$, 5.7 mM $GaCl_3$, 4.48 mM H_2SeO_3, and 240 mM LiCl for $Cu(In,Ga)Se_2$. All chemicals were 99.999 % pure and supplied by Alfa Aesar or Sigma-Aldrich unless otherwise stated. The counter and reference electrode were a platinum foil and a silver chloride electrode respectively. The normal deposition procedure consisted of applying a potential of -0.476 V for one minute and then subsequently washing and drying the film before placing it back into the deposition bath where a further deposition was continued for 70 minutes, with the last 50 minutes at -0.576 V. The films were annealed in 10% H_2, 90% N_2 at 10 mbar atmosphere at 550°C for thirty minutes, in the presence of excess selenium. These electrodeposited and annealed films will be referred to as ED-$CuInSe_2$ and ED-$Cu(In,Ga)Se_2$, respectively.

For comparison with the electrodeposited material, other $CuInSe_2$ films were deposited by a 2-stage processing by means of selenisation of metallic CuIn precursor on Mo-coated soda-lime glass substrates. The substrates were cleaned in an ultrasonic bath using i) Decon90 solution, ii) distilled water and iii) isopropanol and then blown dry in nitrogen. An 800 nm thick Mo film was radio frequency (RF) magnetron sputtered onto the substrate followed by RF magnetron sputtering from high purity 5N targets of Cu and In elements. The substrates were rotated to ensure uniformity of the deposition. The precursor films consisted of alternate deposition of 240 single Cu and In layers with a total thickness of ~800 nm. Selenium was then thermally evaporated and selenisation completed in a tube furnace in Ar and Se atmosphere at temperature of 500ºC for 30 min. The final thickness of the $CuInSe_2$ film was ~1500 nm. Two sputtered and annealed films were used as comparison materials, and these are referred to as SP1-$CuInSe_2$ and SP2-$CuInSe_2$, respectively.

$CuInS_2$ films were produced using a novel electrostatic spray deposition technique that uses a high potential difference between a nozzle outlet and the substrate to generate an aerosol that deposits thin films onto the heated substrate. A water/alcohol solution was prepared dissolving $CuCl_2$ (99.99% Aldrich), $InCl_3$ (99.99%, Alfa Aesar), and thiourea (99+%, Alfa Aesar). The copper concentration was fixed at 30 mM while the S/Cu and Cu/In ratios were respectively maintained at 5 and 1. The precursor solution was pumped through the nozzle to deposit the films. In this experiment the solution was sprayed at 50 $\mu L.min^{-1}$ across potential difference of 18 kV, with a substrate temperature of 450°C.

The composition and morphology of films were analyzed using a JEOL JSM6310 scanning electron microscope (SEM) with energy dispersive X-ray analyzer (EDAX). X-ray diffraction (XRD) measurements were carried out with a Philips PW1820/00 diffractometer. Photoelectrochemical measurements of copper chalcopyrite films were performed in aqueous 0.2 M europium nitrate (99.9%, Strem) saturated in potassium perchlorate (99.5%, Fluka), adjusted to pH 2 by nitric acid. Samples were etched in 5 wt% potassium cyanide (98%, Fluka). Measurements were carried out in a three electrode configuration using a glass cell with a Ag|AgCl reference electrode, and a platinum foil as a counter electrode. Cyclic voltammograms and constant potential photocurrent transients of the films were recorded using an Autolab 20 potentiostat under pulsed 520 nm green light illumination provided by a light emitting diode (LED). Photocurrent spectra were recorded with a standard photoelectrochemical setup: lamp, monochromator, and chopper (Bentham); purpose-built potentiostat, function generator (Hi-Tek); lock-in amplifier (Stanford Research Systems). Spectra were recorded using chopped illumination with a frequency of 13 Hz or higher and normalized against calibrated silicon and germanium photodiodes.

Results and Discussion

Materials Characterization

The appearance of the as-deposited ED-$CuInSe_2$ films varied depending on the number of samples previously plated. The first deposited film formed a smooth compact reflective grey layer. Films deposited subsequently from the same solution grew darker in color and developed rough surfaces, with particles visible to the eye. As-deposited ED-$Cu(In,Ga)Se_2$ films always appeared highly reflective and slightly darker than the

ED-$CuInSe_2$ films. SEM measurements showed the as-deposited films to be approximately 2 μm thick. Figures 1A and 1B show SEM images of the sixth as-deposited films grown in a series from the same bath for both ED-$CuInSe_2$ and ED-$Cu(In,Ga)Se_2$ films, respectively. The ED-$CuInSe_2$ shows a compact layer with dendrites projecting from the surface. EDAX measurements showed that the bulk of the film is slightly copper poor with a film composition of 22 at% Cu, 23.5 at% In, 51.5 at% Se and 3 at% oxygen. The composition of the dendrites is slightly indium poor compared to the bulk of the film. The ED-$Cu(In,Ga)Se_2$ layer is smoother with fewer dendrites on the surface. The bulk film composition is 21 at% Cu, 15.5 at% In, 4.9 at% Ga, 45.2 at% Se and 13.4 at% oxygen, suggesting that most of the gallium is present as $Ga(OH)_3$. Figures 1C and 1D show SEM images of the annealed ED-$CuInSe_2$ and ED-$Cu(In,Ga)Se_2$ films, respectively. The annealed ED-$CuInSe_2$ film appears to be rougher and has several cracks. By contrast, the annealed $Cu(In,Ga)Se_2$ film appears smooth and compact as a whole with some small crystals. DAX measurements show that annealing in hydrogen reduce the oxygen content from 13.4 to 0.9 at%. EDAX measurements reveal that the bulk of the film contains gallium but the small crystals do not, suggesting that some segregation of gallium occurs during the annealing process. Calixto *et al.* did not report segregation of gallium, but this may be because their films were annealed in H_2Se gas, and not elemental selenium and H_2 gas (4).

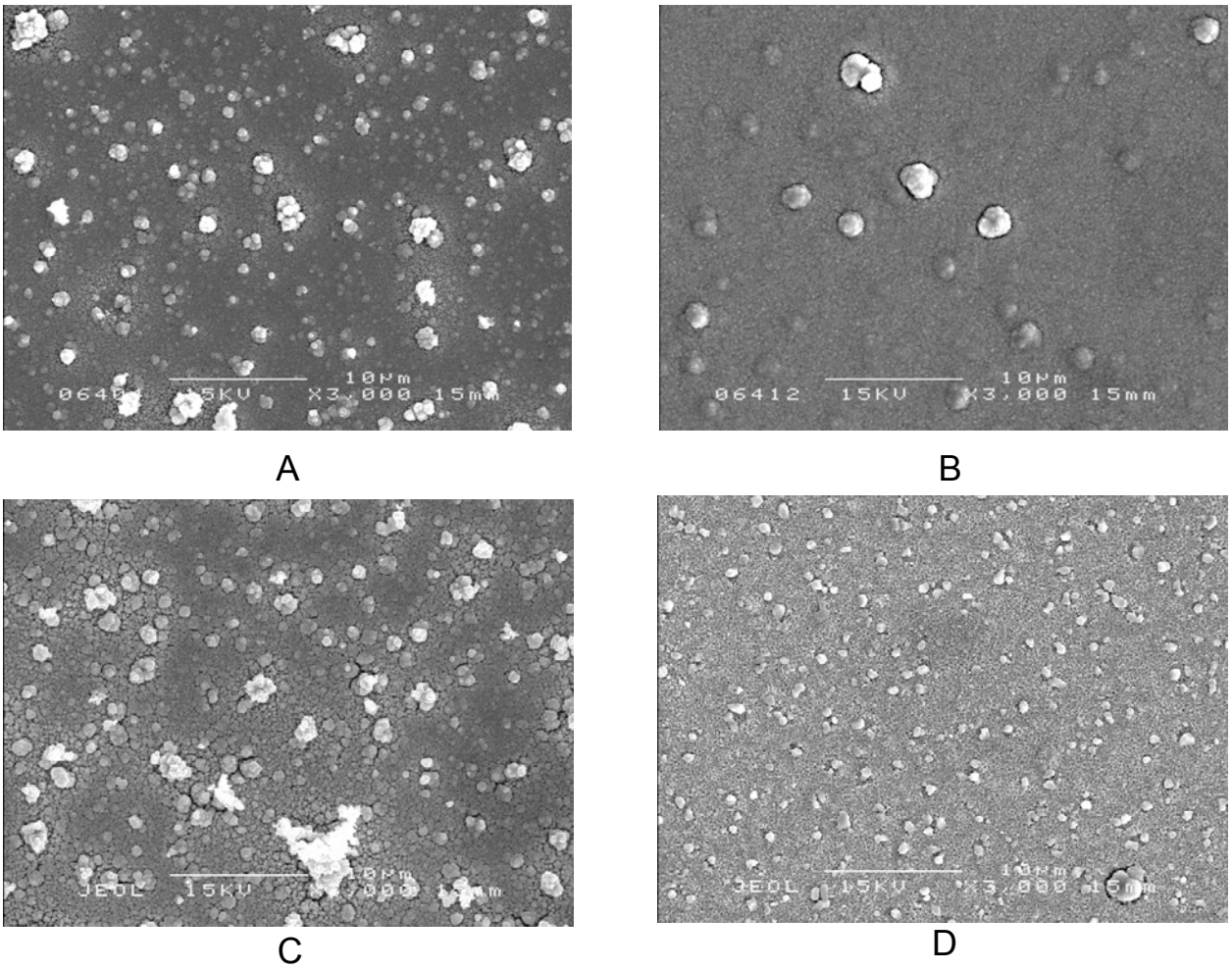

Figure 1. SEM images of ED-$CuInSe_2$ as-deposited (A) and annealed (C), and ED-$Cu(In,Ga)Se_2$ as deposited (B) and annealed (D).

Figure 2 shows the XRD spectra of ED-$CuInSe_2$ films before and after annealing. The as-deposited material displays the three main $CuInSe_2$ peaks; (112), (220/204), and (312/116), although the peaks are rather broad and weak indicating poor crystallinity. Annealing the ED-$CuInSe_2$ crystallizes the as-deposited film to produce larger grain sizes, giving well defined sharp peaks in the XRD spectra. All the peaks are identifiable and attributable to $CuInSe_2$ chalcopyrite phase and the only secondary phase observed is $MoSe_2$, which is formed during the annealing process when the temperature is taken above 450ºC (15). XRD spectra of $Cu(In,Ga)Se_2$ films were also recorded, however no characteristic shift in the chalcopyrite peaks due to the gallium content could be discerned.

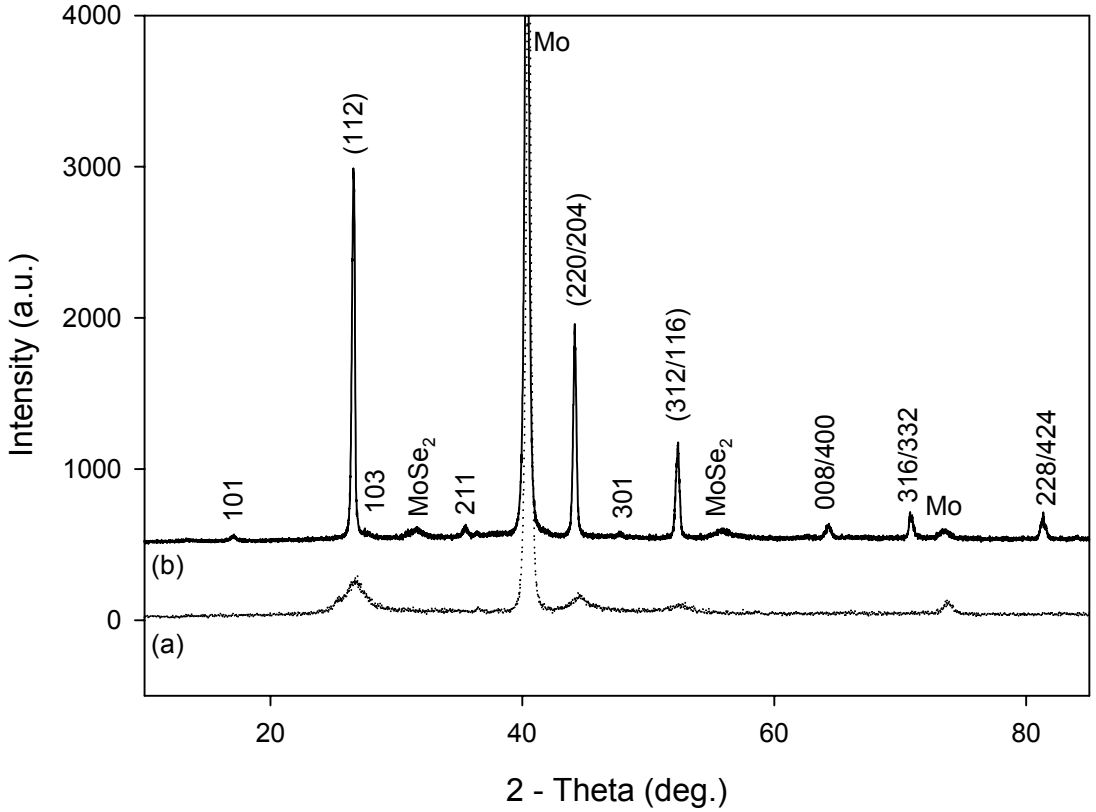

Figure 2. XRD patterns of (a) as deposited and (b) annealed ED-$CuInSe_2$ films.

Opto-electronic Characterization

An important step in making chalcopyrite based absorber layer photovoltaic devices is the cyanide etch that is used before depositing the buffer layer. This etch is believed to remove excess copper and selenium phases from the surface, leaving it indium rich (16). Figure 3 shows how the normalized photocurrent response to a constant light stimulus varies as a function of etch time for ED-$CuInSe_2$ and SP1-$CuInSe_2$ films held at -0.3 V. It can be seen that the two films respond differently. The ED-$CuInSe_2$ film exhibits a large photocurrent before any etching,. The photocurrent then diminishes after 45 s of etching, but then returns to its initial value after 90 s of etching. In contrast, SP1-$CuInSe_2$ shows no photocurrent before etching, but the photocurrent then increases steadily with etch time, reaching a maximum after etching for 140 s. It was also noted for both films

that the dark current decreased to a low and steady plateau with increased etch time. In the case of the fresh sprayed $CuInS_2$ samples, etching had no influence on the photocurrent response.. However, after the films had been left for a week in air, the photocurrent performance was reduced considerably, and in this case a five second dip in KCN solution sufficed to restore the original response.

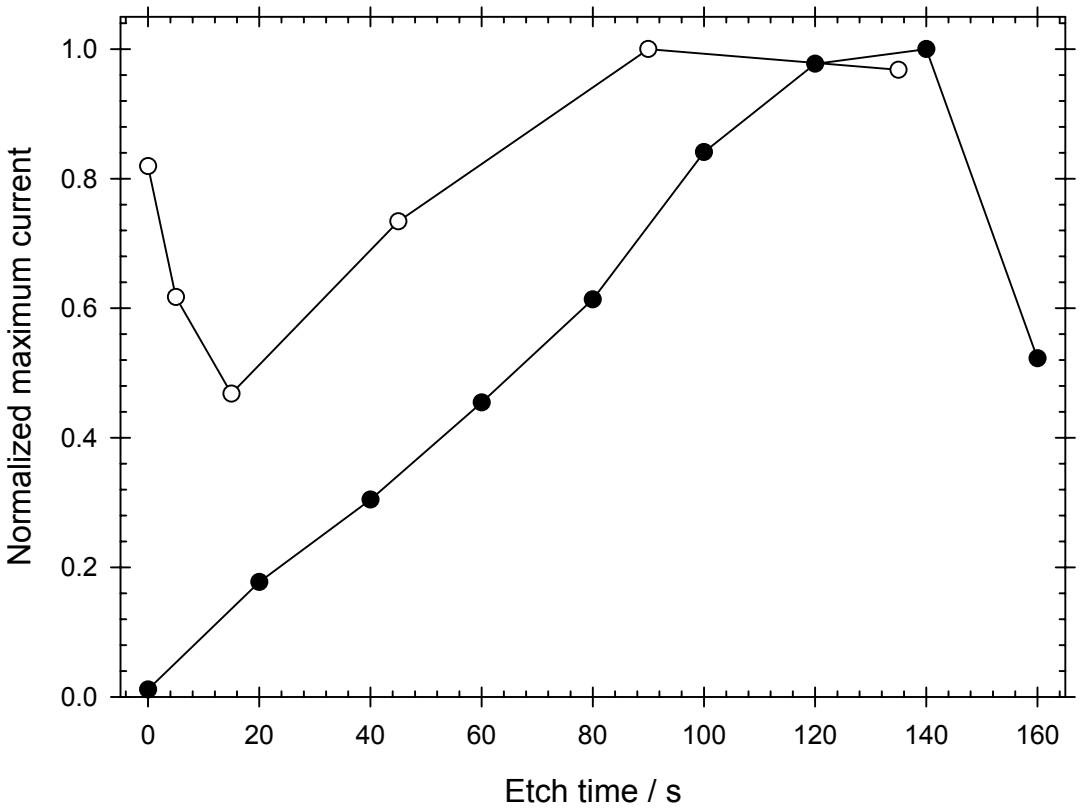

Figure 3. Graph showing normalized photocurrent response to pulsed green LED illumination for ED-$CuInSe_2$ (○) and SP-$CuInSe_2$ (●) films. All photocurrents were measured at –0.3 vs Ag|AgCl / V in aqueous 0.2 M Eu^{3+} electrolyte at pH 2.

.

Figure 4 shows a forward scan of a photovoltammogram measured for an ED-$CuInSe_2$ film after it had been etched in KCN for 90 s. The potential was swept from 0 V to –0.5 V at 20 $mV.s^{-1}$ whilst illuminating the sample with a pulsed green light LED (on time 0.4 s and off time 1 s). A cathodic photocurrent (i.e. p-type) response is observed, which begins at approximately –0.1 V and increases as the potential is made more negative.. The dark current starts to rise around –0.4 V, indicating reduction of the film. Illumination generates minority carriers (electrons) in the conduction band, which can either be scavenged by the Eu^{3+} ions in solution, or trapped at surface recombination sates, leading to recombination. At small applied negative potentials, where the band bending and space charge region at the film/solution interface are small, recombination si dominant so that the observed photocurrent is small. At more negative potentials, recombination is less important minority carriers are be scavenged more effectively by Eu^{3+} ions. No saturation of the photocurrent was observed in the limited measured potential range.

Qualitatively, a 140 s etched SP-$CuInSe_2$ film shows the same characteristics as the electrodeposited film, but the onset of the photocurrent is shifted to 0 V, indicating a slightly more positive flat band potential or less recombination. Lincot *et al*. found that the flat band position for co-evaporated $CuInSe_2$ films depended on the degree of surface oxidation and illumination intensity, with a higher level of oxidation giving a more positive flat band potential and light illumination giving a more negative flat band potential (12). An un-etched $CuInS_2$ film also shows a negative photocurrent, with the onset potential shifted to –0.2 V.

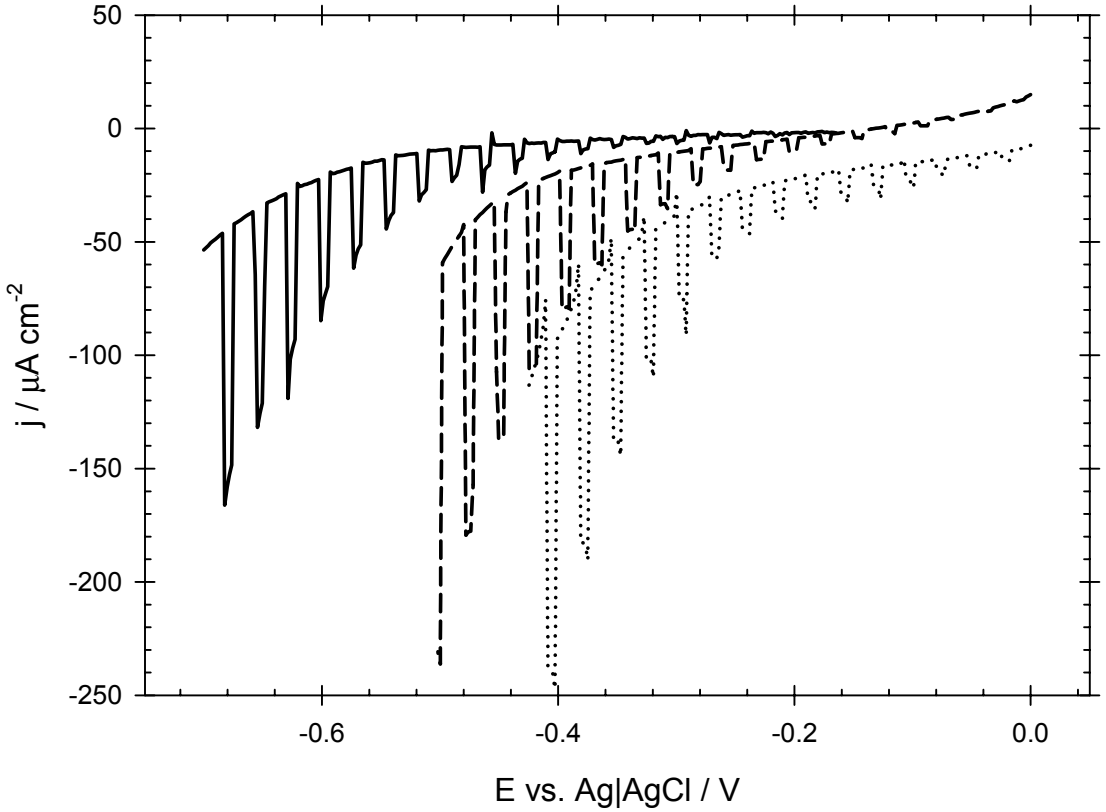

Figure 4. Photovoltammograms of $CuInS_2$ (—), ED-$CuInSe_2$ (--), and SP-$CuInSe_2$ (····). All films were contacted with aqueous 0.2 M Eu^{3+} electrolyte at pH 2. LED illumination on for 0.4 s and off for 1 s. Scan rate 20 $mV.s^{-1}$.

The photocurrent transient response to pulsed green light on ED-$CuInSe_2$ film was recorded at a fixed potential of –0.3 V, and the response to one pulse is shown in figure 5. For comparison the response of a silicon photodiode is also shown.. The films were illuminated between 0.25 and 0.65 s.. The photoresponse of ED-$CuInSe_2$ (figure 5b) to the illumination shows an instantaneous negative current spike that decays to a constant negative current. When the illumination is interrupted, a positive current spike is observed which decays quickly to the background dark current. A negative photocurrent is consistent with a p-type semiconductor, which is also observed for SP1-$CuInSe_2$ (figure 5c). Small negative photocurrents were observed for ED-$Cu(In,Ga)Se_2$ with much slower rise times than for other films.

Figure 6A illustrates the effect of applied potential on the photocurrent transient response of an ED-$CuInSe_2$ film that had been KCN etched for 90 s. At –0.2 V, a small photocurrent response is observed that decays quickly to a steady state with time and then

an opposite positive current response is observed when the light is switched off. As the potential is made more negative, the instantaneous photocurrent response increases, the decay to the steady state takes longer and the magnitude of the steady state current is also higher. The magnitude of the positive photocurrent also decreases with increasing negative applied potentials. Similarly figure 6B demonstrates the same effects but for an un-etched $CuInS_2$ film. Here the shape of the photocurrent response appears offset by -0.1 V, probably due to the different flat band potentials of the two materials.

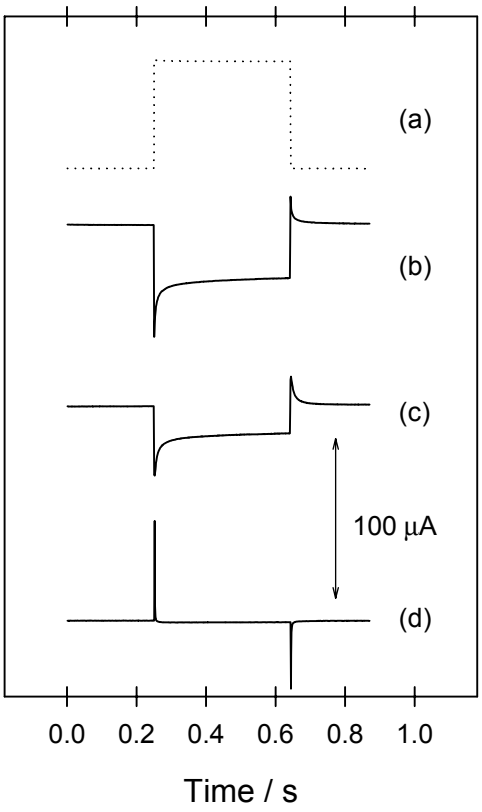

Figure 5. Photocurrent transient response to a pulsed 520 nm green LED of (a) a silicon photodiode, (b) ED-$CuInSe_2$ film, (c) SP1-$CuInSe_2$ and (d) SP2-$CuInSe_2$ films. All films had a potential of –0.3 vs Ag|AgCl / V applied in aqueous 0.2 M Eu^{3+} electrolyte at pH 2.

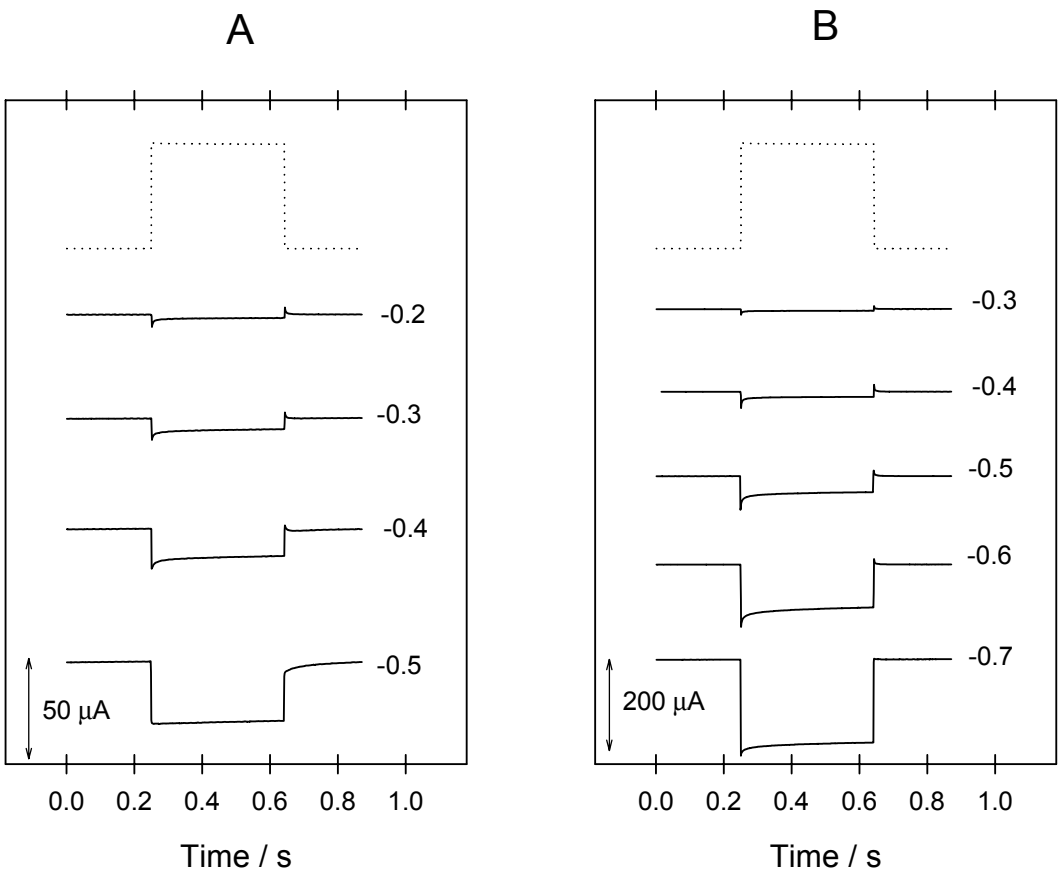

Figure 6. Photocurrent transient response to pulsed green LED at different applied potentials for ED-$CuInSe_2$ (A) and $CuInS_2$ (B) films. Numbers at the side indicate applied potential vs. Ag|AgCl / V in Eu^{3+} at pH 2. Dotted line represents the current response of silicon photodiode.

The shape of the photocurrent transients at fixed voltages is attributable to the two competing processes occurring at the film/electrolyte interface. The negative current is due to the reduction of the Eu^{3+} ions in solution by minority carriers as outlined above. The positive current is due to the fact that even when there is no illumination, the trapped minority carriers (electrons) in surface states are still recombining with the majority carriers (holes) At low negative potentials the recombination with majority carriers predominates, whilst at high negative potentials the reduction of the Eu^{3+} ions predominates.

Figure 5d is a photocurrent transient of SP2-$CuInSe_2$ which has the same composition as the previous film. However, it produces a positive photocurrent under illumination that very quickly decays to a small negative current. When the illumination stops there is a large negative current response, and the current returns to a small positive value. A positive photocurrent is characteristic of an n-type semiconductor, where the holes are collected at the electrolyte interface. In this case Eu^{3+} ions cannot scavenge the holes and so the photocurrent very quickly decays, probably as a consequence of photo-oxidation of the surface.

The XRD spectra of SP1 and SP2-$CuInSe_2$ films are shown in figure 7a and figure 7b, respectively. For SP1-$CuInSe_2$ the peaks observed correspond to the Mo film and to the

$CuInSe_2$ chalcopyrite phase except for one extra peak at $2\theta = 24.2°$ identified as the commonly observed α-$CuSe_2$ phase. SP2-$CuInSe_2$ was grown under similar conditions to SP1-$CuInSe_2$ but the XRD spectra show the presence of some extra phases in the film, such as indium selenide, and also copper indium alloy phases. The presence of these phases is attributed to incomplete conversion of the precursor during the selenisation of the copper indium alloy precursor. Indium selenide is a n-type semiconductor and is likely to be the reason for the photocurrent response observed. The steady state illumination of SP2-$CuInSe_2$ produces a small negative photocurrent consistent with some p-type chalcopyrite material also being present.

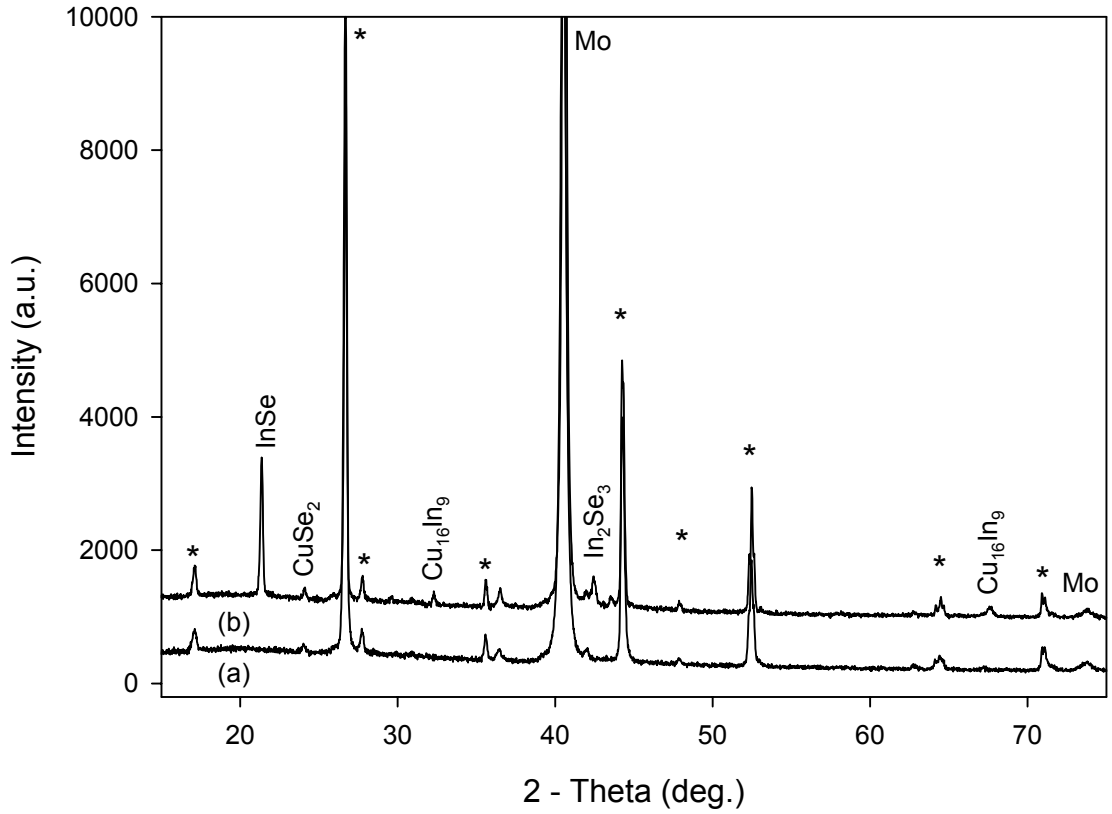

Figure 7. XRD spectra of SP1-$CuInSe_2$ (a) and SP2-$CuInSe_2$ (b). Regular $CuInSe_2$ phases are denoted with a star and the extra phases observed are labeled accordingly.

(IPCE) spectra for each of the films are shown in figure 8. The ED-$CuInSe_2$ film demonstrates a maximum IPCE of 55 % compared to 70 % for the SP-$CuInSe_2$ film, but the IPCE drops off quite rapidly at longer wavelengths, probably indicating that the sample is probably quite highly doped. The sample has a band gap of 0.95 eV, which is slightly lower than that of the SP1-$CuInSe_2$ film, which has a band gap of 1 eV. The ED-$Cu(In,Ga)Se_2$ sample has a poor efficiency with no evidence of the expected band gap shift to shorter wavelengths expected for a film with 5 % gallium doping. This is further evidence that gallium was not incorporated successfully into the chalcopyrite structure. The $CuInS_2$ sample also shows sloping response above the bandgap, again suggesting high doping, and the band edge at 1.1eV indicates considerable sub band gap response. However, when photocurrent spectra are measured for $CuInS_2$ grown on to a cadmium sulphide layer, the $CuInS_2$ has a normal band gap of 1.5 eV.

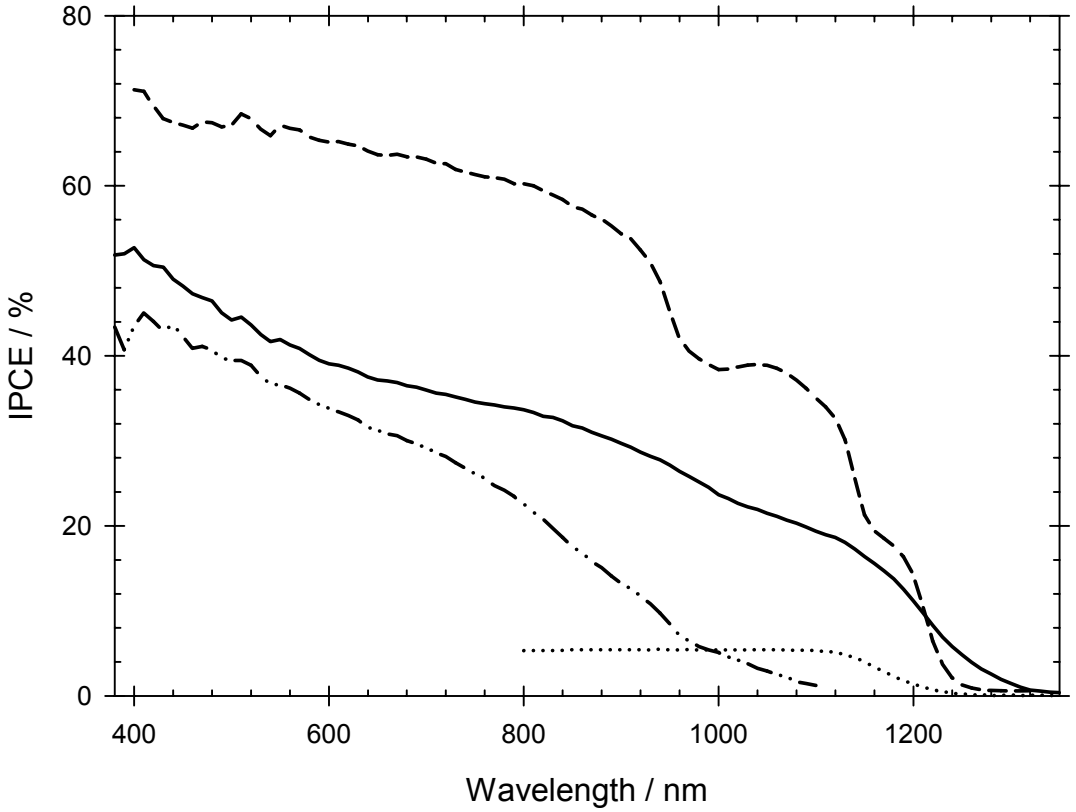

Figure 8. IPCE spectra of ED-$CuInSe_2$ (—), ED-$Cu(In,Ga)Se_2$ (····), SP-$CuInSe_2$ (---), and $CuInS_2$ (-··-). Applied potentials and chopping frequencies were optimised to give the maximum photo-response. All films were measured in 0.2 M Eu^{3+} solution.

The best ED-$CuInSe_2$ layers were converted into full devices by deposition fabrication of cadmium sulphide, zinc oxide, and indium doped tin oxide layers. They gave a conversion efficiency of 4.5 % as compared to the Calixto *et al.* best performance of 6.5 % (4).

Conclusions

Photocurrent measurements with electrolyte contacts provide a convenient tool for screening and optimization of the preparation of chalcopyrite absorber films for thin film solar cells. The measurements have allowed optimum deposition an etching times to be established.

Acknowledgements

This work was funded by the EPSRC through the Supergen programme: PV for the 21st Century. The authors would like to thank Hugh Perrot and Barry Chapman for SEM and XRD measurements.

References

1. M. A. Contreras, K. Ramanathan, J. AbuShama, F. Hasoon, D. Young, B. Egass, and R. Noufi, *Prog. Photovoltaics*, **13,** 209 (2005).
2. J. Palm, V. Probst, A. Brummer, W. Stetter, R. Tolle, T. P. Niesen, S. Visbeck, O. Hernandez, M. Wendl, H. Vogt, H. Calwer, B. Freienstein and F. Karg, *Thin Solid Films*, **431**, 514 (2003)
3. D. Cunningham, M. Rubcich and D. Skinner, *Prog. Photovoltaics*, **10**, 159 (2002).
4. M. E. Calixto, K. D. Dobson, B. E. McCandless and R. W. Birkmire, *J. Electrochem. Soc.*, **153**, G521 (2006).
5. D. Lincot, J. F. Guillemoles, S. Taunier, D. Guimard, J. Sicx-Kurdi, A. Chaumont, O. Roussel, O. Ramdani, C. Hubert, J. P. Fauvarque, N. Bodereau, L. Parissi, P. Panheleux, P. Fanouillere, N. Naghavi, P. P. Grand, M. Benfarah, P. Mogensen and O. Kerrec, *Sol. Energy*, **77**, 725 (2004).
6. S. Nomura, K. Nishiyama, K. Tanaka, M. Sakakibara, M. Ohtsubo, N. Furutani and S. Endo, *Jpn. J. Appl. Phys. Part 1 - Regul. Pap. Short Notes Rev. Pap.*, **37**, 3232 (1998).
7. G. Hodes, T. Engelhard, D. Cahen, L. L. Kazmerski and C. R. Herrington, *Thin Solid Films*, **128**, 93 (1985).
8. A. Kampmann, J. Rechid, A. Raitzig, S. Wulff, R. Mihhailova, R. Thyen and K. Kalberlah, *Proceeding of the MRS Spring Meeting* (2003).
9. Y. W. Chen, D. Cahen, R. Noufi and J. A. Turner, *Solar Cells*, **14**, 109 (1985).
10. T. Wilhelm, B. Berenguier, M. Aggour, K. Skorupska, M. Kanis, M. Winkelnkemper, J. Klaer, C. Kelch and H.-J. Lewerenz, *Thin Solid Films*, **480-481**, 24 (2005).
11. D. Cahen, Y. W. Chen, R. Noufi, R. Ahrenkiel, R. Matson, M. Tomkiewicz and W. M. Shen, *Solar Cells*, **16**, 529 (1986).
12. D. Lincot, H. G. Meier, J. Kessler, J. Vedel, B. Dimmler and H. W. Schock, *Solar Energy Materials*, **20**, 67 (1990).
13. S. Menezes, J. F. Guillemoles, B. Canava, J. Vedel and D. Lincot, in *Conference Record of the Twenty Sixth IEEE Photovoltaic Specialists Conference*, 411 (1997).
14. D. Guimard, P. P. Grand, N. Bodereau, P. Cowache, J. F. Guillemoles, D. Lincot, S. Taunier, M. Ben Farah and P. Mogensen, in *Conference Record of the Twenty-Ninth IEEE Photovoltaic Specialists Conference* . 692 (2002).
15. M. E. Calixto, K. D. Dobson, B. E. McCandless and R. W. Birkmire, in *Conference Record of the Thirty-First IEEE Photovoltaic Specialists Conference* 378 (2005).
16. M. Kemell, M. Ritala and M. Leskela, *Crit. Rev. Solid State Mat. Sci.*, **30**, 1 (2005).